



ELSEVIER

Contents lists available at ScienceDirect

Neuropharmacology

journal homepage: www.elsevier.com/locate/neuropharm

Inhibiting the interaction between apoptosis-inducing factor and cyclophilin A prevents brain injury in neonatal mice after hypoxia-ischemia

Juan Rodriguez^a, Cuicui Xie^a, Tao Li^{a,b,c}, Yanyan Sun^{a,b,d}, Yafeng Wang^{a,b,c}, Yiran Xu^{a,b}, Kenan Li^{a,b}, Shan Zhang^{a,b}, Kai Zhou^{a,b,e}, Yong Wang^{a,b}, Carina Mallard^{b,f,g}, Henrik Hagberg^{f,h}, Nunzianna Dotiⁱ, Xiaoyang Wang^{b,f,g}, Changlian Zhu^{a,b,e,f,*}

^a Center for Brain Repair and Rehabilitation, Institute of Neuroscience and Physiology, Sahlgrenska Academy, University of Gothenburg, Gothenburg, 40530, Sweden

^b Henan Key Laboratory of Child Brain Injury, Institute of Neuroscience and Third Affiliated Hospital of Zhengzhou University, Zhengzhou, 450052, China

^c Department of Pediatrics, Children's Hospital of Zhengzhou University, Zhengzhou, China

^d Department of Anatomy, School of Basic Medical Science, Zhengzhou University, Zhengzhou, 450001, China

^e Department of Women's and Children's Health, Karolinska Institutet, Stockholm, Sweden

^f Centre of Perinatal Medicine and Health, Sahlgrenska Academy, University of Gothenburg, Gothenburg, Sweden

^g Institute of Neuroscience and Physiology, Sahlgrenska Academy, University of Gothenburg, Gothenburg, 40530, Sweden

^h Dept of Obstetrics and Gynecology, Institute of Clinical Sciences, Sahlgrenska Academy, University of Gothenburg, Sweden

ⁱ Istituto di Biostrutture e Bioimmagini-CNR, Via Mezzocannone 16, Napoli, 80134, Italy

HIGHLIGHTS

- Apoptotic cell death is more prominent in the immature brain after insult.
- Apoptosis inducing factor (AIF) plays a crucial role in the process of apoptosis in the immature brain after injury.
- AIF induces apoptosis require interaction with cyclophilin A.
- Blocking interaction of AIF and cyclophilin A reduces caspase-independent cell death and brain injury only in males.

ARTICLE INFO

Keywords:

Apoptosis-inducing factor
Blocking peptide
Brain injury
Cyclophilin A
Hypoxia-ischemia
Immature brain

ABSTRACT

The interaction between apoptosis-inducing factor (AIF) and cyclophilin A (CypA) has been shown to contribute to caspase-independent apoptosis. Blocking the AIF/CypA interaction protects against glutamate-induced neuronal cell death *in vitro*, and the purpose of this study was to determine the *in vivo* effect of an AIF/CypA interaction blocking peptide (AIF(370-394)-TAT) on neonatal mouse brain injury after hypoxia-ischemia (HI). The pups were treated with AIF (370-394)-TAT peptide intranasally prior to HI. Brain injury was significantly reduced at 72 h after HI in the AIF(370-394)-TAT peptide treatment group compared to vehicle-only treatment for both the gray matter and the subcortical white matter, and the neuroprotection was more pronounced in males than in females. Neuronal cell death was evaluated in males at 8 h and 24 h post-HI, and it was decreased significantly in the CA1 region of the hippocampus and the nucleus habenularis region after AIF(370-394)-TAT treatment. Caspase-independent apoptosis was decreased in the cortex, striatum, and nucleus habenularis after AIF(370-394)-TAT treatment, but no significant change was found on caspase-dependent apoptosis as indicated by the number of active caspase-3-labeled cells. Further analysis showed that both AIF and CypA nuclear accumulation were decreased after treatment with the AIF(370-394)-TAT peptide. These results suggest that AIF (370-394)-TAT inhibited AIF/CypA translocation to the nucleus and reduced HI-induced caspase-independent apoptosis and brain injury in young male mice, suggesting that blocking AIF/CypA might be a potential therapeutic target for neonatal brain injury.

Abbreviations: AIF, apoptosis-inducing factor; CA1, cornu ammonis area 1; CP, cerebral palsy; CypA, cyclophilin A; HI, hypoxia ischemia; MAP2, microtubule-associated protein 2; MBP, and myelin basic protein; NH, nucleus habenularis; PARP-1, poly (ADP-ribose) polymerase-1

* Corresponding author. Center for Brain Repair and Rehabilitation, Institute of Neuroscience and Physiology, University of Gothenburg, Gothenburg, 40530, Sweden.

E-mail address: changlian.zhu@neuro.gu.se (C. Zhu).

<https://doi.org/10.1016/j.neuropharm.2020.108088>

Received 1 October 2019; Received in revised form 7 March 2020; Accepted 2 April 2020

Available online 08 April 2020

0028-3908/ © 2020 The Authors. Published by Elsevier Ltd. This is an open access article under the CC BY license

(<http://creativecommons.org/licenses/by/4.0/>).

1. Introduction

Perinatal brain injury is an important cause of developmental impairment and of permanent neurological deficits such as cerebral palsy (CP) in children (Novak et al., 2018). The progression of brain injury depends on the balance between persistent injury and the repair response, which can be modulated by external therapies (Fleiss and Gressens, 2012; Hagberg et al., 2016). Recent studies have shown that perinatal asphyxia and preterm birth are the two most common perinatal complications associated with perinatal brain injury (Liu et al., 2016; Strunk et al., 2014). Two significant breakthroughs have been the discoveries that hypothermia and erythropoietin both reduce brain damage and the occurrence of CP after perinatal hypoxia-ischemia (HI) brain injury in term infants and that erythropoietin is protective in very preterm infants (Song et al., 2016; Azzopardi et al., 2014; Zhu et al., 2009). However, these treatments are not successful in all cases (Natalucci et al., 2016), and there is a pressing need for comparative and translational studies to find ways to prevent neuronal cell death and to promote brain repair after perinatal brain injury.

Neuronal cell death after perinatal insults occurs through apoptosis, necrosis, autophagy, ferroptosis, or necroptosis, each of which has distinct morphological characteristics (Thornton et al., 2017; Wu et al., 2019; Xie et al., 2016), and mitochondria are key regulators of neuronal cell death by regulating energy metabolism and the release of cell death-related proteins (Hagberg et al., 2014). It has been shown that apoptosis-inducing factor (AIF), which normally resides in the mitochondria, plays a fundamental role in mitochondrial regulation after HI not only through the loss of the mitochondria's energy-producing function, but also through AIF's release into the cytosol and subsequent translocation into the nucleus where it induces apoptosis through chromatin condensation and large-scale DNA fragmentation in a caspase-independent manner (Zhu et al., 2007a; Klein et al., 2002). This process is more prominent in the immature brain than in the mature brain (Zhu et al., 2005). As an indicator of the importance of this protein, neuron death in the brain after an episode of HI was reduced by 70% in a mouse model with AIF haploinsufficiency (Zhu et al., 2007a; Sun et al., 2012), while in a mouse model with AIF overexpression the infarction volume increased by 75% (Li et al., 2020).

Our previous study showed that AIF-induced neuron death requires AIF binding to cyclophilin A (CypA) in the cytosol and subsequent translocation to the nucleus to induce chromatin degradation (Zhu et al., 2007b), and thus the AIF/CypA complex might be a good candidate for generating a pharmacological inhibitor to block the cell death process (Doti et al., 2014). A specific peptide, based on the AIF and CypA sequences that correspond to the surfaces involved in binding of AIF and CypA, has recently been designed (Farina et al., 2017). The

in vitro experiments demonstrated the efficacy and protective effect of the synthetic peptide, which was able to inhibit AIF/CypA complex formation by competitive binding to CypA and thus caused failure of the translocation of AIF from the cytosol to the nucleus (Doti et al., 2014). The purpose of this study was to investigate whether administration of the AIF blocking peptide *in vivo* has neuroprotective effects in neonatal mice after cerebral HI.

2. Material and methods

2.1. Cerebral hypoxia-ischemia

Postnatal day 9 (P9) C57BL/6J mice (Janvier Labs, France) of both sexes were anesthetized with isoflurane (5% for induction, 1.5%–2.0% for maintenance) in a 1:1 mixture of air and oxygen, and the duration of anesthesia was less than 5 min. The right common carotid artery was cut between double ligatures of Prolene sutures (6.0). After the surgical operation, the wounds were infiltrated with lidocaine for local analgesia. The pups were returned to their cages with their dams for 1 h and then placed in a chamber perfused with a humidified gas mixture (10% oxygen in nitrogen) for 40 min at 36 °C, with 10 min of air before and after as acclimation in the chamber. Following hypoxic exposure, the pups were returned to their cages until being sacrificed (Rodriguez et al., 2018). Mice were maintained in the Laboratory for Experimental Biomedicine of Gothenburg University, and all of the experiments were performed in accordance with national guidelines and approved by the Gothenburg Animal Ethics Committee (112/2014).

2.2. Intranasal AIF(370-394)-TAT peptide administration

AIF/CypA interaction blocking peptide (AIF(370-394)) conjugated at N-terminus with the TAT sequence (hereafter AIF(370-394)-TAT) was synthesized as described previously (Doti et al., 2014). P9 mouse pups were first pretreated with 1 drop of 1.5 µl hyaluronidase Type IV-S (10 mg/ml = 10,000 U/ml) (Sigma, H4272) in both nostrils. At the time the pups were pretreated and immediately before the operation for the ligation of the carotid artery, 1.5 µl of the AIF(370-394)-TAT peptide at a concentration of 5 µg/µl was administered to both nostrils in the treated mice, and the same amount of vehicle was administered to both nostrils in the vehicle-treated mice (Albertsson et al., 2014). Pups were firmly held in the hand in a supine position until the drug was completely inhaled and the nostrils were dry. The pups were put back with their dam for 1 h after the operation, and the peptide was administered again just before exposure to hypoxia. For the mice that were used for microtubule-associated protein 2 (MAP2) and myelin basic protein (MBP) staining 72 h after the insult, hyaluronidase and AIF(370-394)-TAT were also administered at 12 h post HI (Fig. 1).

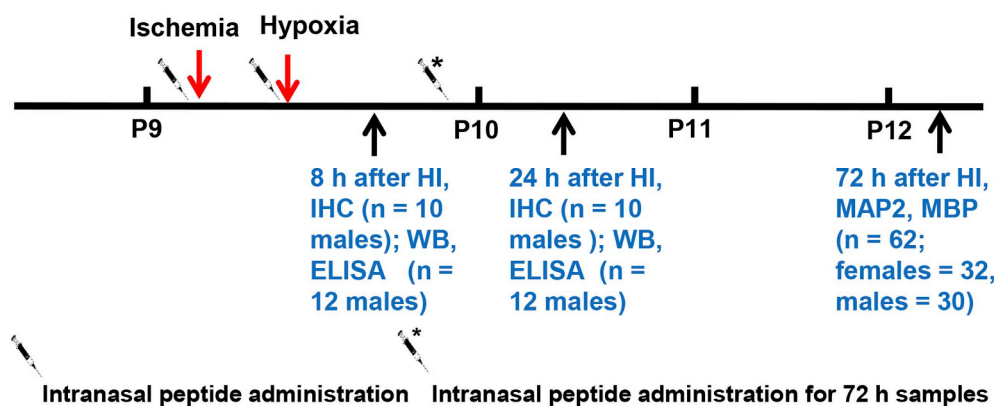


Fig. 1. The study design. The AIF(370-394)-TAT peptide was administered intranasally immediately prior to the induction of ischemia and hypoxia on P9. At 8 h after HI, 10 male pups (5 AIF-TAT and 5 Veh mice) were perfused for immunostaining and 12 male pups (6 AIF-TAT and 6 Veh mice) were perfused for ELISA and Western blot. At 24 h after HI, a further 10 male pups (5 AIF-TAT and 5 Veh mice) were perfused for immunohistochemistry staining and 12 male pups (6 AIF-TAT and 6 Veh mice) were perfused for ELISA and Western blot. At 72 h after HI, 62 pups were perfused for MAP2 and MBP staining to evaluate brain injury – 31 mice (16 females and 15 males) were treated with the AIF(370-394)-TAT peptide, and 31 mice (16 females and 15 males) were treated with vehicle and used as controls.

2.3. Immunohistochemistry staining

At 8 h, 24 h, or 72 h after HI, the pups were deeply anesthetized with 50 mg/ml phenobarbital and perfused intracardially with PBS and 5% buffered formaldehyde (Histofix; Histolab, Gothenburg, Sweden). Brains were carefully separated from the skulls, and the cerebellums were cut off in a coronal plane. The brains were fixed in 5% buffered formaldehyde at 4 °C for 18–24 h. After dehydration with graded ethanol and xylene, the brains were paraffin-embedded and cut into 5 µm coronal sections. For samples taken at 72 h after HI, every 100th section throughout the whole brain was stained for MAP2 and MBP. For samples taken at 8 h and 24 h after HI, every 50th section in the hippocampus level was stained for active caspase-3, AIF, and Fluoro-Jade. Briefly, the immunohistochemical staining was performed as follows. Sections were deparaffinized in xylene and rehydrated in graded ethanol concentrations. Antigen retrieval was performed by heating the sections in 10 mM boiling sodium citrate buffer (pH 6.0) for 10 min. Nonspecific binding was blocked for 30 min with 4% donkey or goat serum in PBS for 30 min. The primary antibodies were monoclonal mouse anti-MAP2 (1:1,000 dilution, clone HM-2, Sigma, M4403), polyclonal rabbit cleaved caspase-3 (1:300 dilution, Asp175, Cell Signaling, 9661), monoclonal rabbit anti-AIF (1:500 dilution, E20, Abcam, ab32516), monoclonal mouse anti-MBP (1:400 dilution, clone SMI94, BioLegend, 836504), and rat anti-galectin 3 (1:300, Clone: eBioM3/38, Cat: 14-5301, eBioscience). After incubating the sections with the primary antibodies overnight at 4 °C, the appropriate biotinylated secondary antibodies (1:200 dilutions; all from Vector Laboratories, Burlingame, CA, USA) were added for 60 min at 21 °C. After blocking endogenous peroxidase activity with 3% H₂O₂ for 10 min, the sections were visualized with Vectastain ABC Elite (Vector Laboratories) and 0.5 mg/ml 3,3'-diaminobenzidine enhanced with ammonium nickel sulfate, β-D glucose, ammonium chloride, and β-glucose oxidase. After dehydrating with graded ethanol and xylene, the sections were mounted using Vector mounting medium.

2.4. Fluoro-Jade staining

The Fluoro-Jade staining was as previously described, except that after rehydration the samples were incubated in 0.06% potassium permanganate (KMnO₄) for 15 min at room temperature in a shaker and then stained with 0.0004% Fluoro-Jade B (2210364, Temecula, CA, USA) in 0.09% acetic acid for 30 min in the dark. Sections were washed in distilled water twice for 1 min and coverslipped and kept in the dark (Sun et al., 2017).

2.5. Brain injury evaluation

Brain injury was evaluated from eight serial sections per animal based on the infarction volume and the neuropathological scoring, which were based on MAP2 immunostaining and which were performed by a person who did not have prior knowledge of the groups. The MAP2-positive and negative areas in each section were measured in both hemispheres using Micro Image (Olympus, Japan). The infarction volume was calculated from the MAP2-negative areas according to the Cavalieri principle using the following formula: $V = \Sigma A \times P \times T$, where V = the total volume, ΣA = the sum of area measurements, P = the inverse of the sampling fraction, and T = the section thickness. The neuropathological score of gray matter from different brain regions was assessed. Briefly, the cortical injury was graded from 0 to 4 with 0 being no observable injury and 4 indicating confluent infarction. The injury in the hippocampus, striatum, and thalamus was assessed both with respect to hypotrophy (scored from 0 to 3) and injury/infarction (scored from 0 to 3), resulting in a total possible score of 22. Regarding MBP staining, the subcortical white matter of both hemispheres was measured using Image J 1.52a software (NIH, Bethesda, MD; <http://rsb.info.nih.gov/ij>), and the final result was calculated by dividing the MBP-positive area in the ipsilateral hemisphere by the MBP-positive area in the contralateral hemisphere. For each animal, three consecutive sections on the same level were calculated and averaged as the final ratio (Li et al., 2019).

Area contours were drawn and measured in every 50th section. The active caspase-3 positive cells, AIF-positive nuclei, and Fluoro-Jade-labeled cells were counted at 200 × magnification in the striatum, hippocampal cornu ammonis area 1 (CA1), and nucleus habenularis (NH). The border zone of the injured cortex was counted at 100 × magnification. Galectin-3-positive cells in the cortex and striatum were counted at 100 × magnification. The regions were counted at the same location through all of the brains. All of the regions were counted using Image J 1.52a software (NIH, Bethesda, MD; <http://rsb.info.nih.gov/ij>), and four sections were counted from each brain with an interval of 250 µm.

2.6. Cell counting

Area contours were drawn and measured in every 50th section. The active caspase-3 positive cells, AIF-positive nuclei, and Fluoro-Jade-labeled cells were counted at 200 × magnification in the striatum, hippocampal cornu ammonis area 1 (CA1), and nucleus habenularis (NH). The border zone of the injured cortex was counted at 100 × magnification. Galectin-3-positive cells in the cortex and striatum were counted at 100 × magnification. The regions were counted at the same location through all of the brains. All of the regions were counted using Image J 1.52a software (NIH, Bethesda, MD; <http://rsb.info.nih.gov/ij>), and four sections were counted from each brain with an interval of 250 µm.

2.7. Western blot analysis

The pups were sacrificed by decapitation at 8 h or 24 h after HI. Tissue from the cortex (including the hippocampus) in each hemisphere was rapidly dissected out on a bed of ice and homogenized immediately using a 2 ml Dounce tissue grinder set (Sigma, D8938), and isolation buffer was added (15 mM Tris-HCl, pH 7.6, 320 mM sucrose, 1 mM dithiothreitol, 1 mM MgCl₂, 3 mM EDTA-K, and 0.5% protease inhibitor cocktail (Sigma P8340), which was made fresh immediately prior to use). Half of the homogenates were aliquoted and stored at –80 °C, and the other half were centrifuged at 800 ×g at 4 °C for 10 min. The pellet was washed, re-centrifuged, and saved as the nuclear fraction. The supernatants were further centrifuged at 9,200 ×g for 15 min at 4 °C, producing mitochondrial and synaptosomal fractions in the pellet and crude cytosolic fractions in the supernatants. The enriched mitochondrial fraction was washed and centrifuged. All fractions were stored at –80 °C.

The protein concentration was determined using the bicinchoninic acid method. A total of 65 µl of each nuclear fraction and mitochondrial fraction sample was mixed with 25 µl NuPAGE LDS 4 × sample buffer (ThermoFisher Scientific, NP0007) and 10 µl reducing agent and then heated at 70 °C for 10 min. Individual samples were run on 4–12% NuPAGE Bis-Tris gels (Invitrogen, NP0336BOX) and transferred to reinforced nitrocellulose membranes (Bio-Rad, 162-0112). The membranes were first blocked with 30 mM Tris-HCl (pH 7.5), 100 mM NaCl, and 0.1% Tween 20 (TBST) containing 5% fat-free milk powder for 1 h at 21 °C, and afterwards the membranes were incubated with rabbit anti-AIF (1:1,000 dilution, E20, Abcam, ab32516), anti-CypA (1:1,000 dilution, rabbit polyclonal antibody, BIOMOL Research Laboratories, Inc.), mouse anti-cytochrome c (1:500, 6H2, Santa Cruz, sc-13561), mouse anti-CHCHD4 (1:200, C-12, Santa Cruz, sc-365137), total oxidative phosphorylation system rodent Western blot mouse antibody cocktail (MS604, 1:250, MitoSciences, Eugene), mouse anti-VDAC1 (1:500 dilution, B-6, Santa Cruz, sc-390996), anti-actin (1:200, rabbit polyclonal antibody, Sigma) or anti-Lamin-B (1:200 dilution, M-20, Santa Cruz, sc-6217, used as the loading control) primary antibodies overnight at 4 °C. After washing (three times for 5 min each in TBST), the membranes were incubated for 60 min at 21 °C with peroxidase-labeled goat anti-rabbit IgG antibody (1:2,000 dilution, Vector, PI-1000) for AIF or with peroxidase-labeled horse anti-goat IgG antibody (1:2,000 dilution, Vector, PI-9500) for Lamin-B. Immunoreactive species were visualized using the SuperSignal West Pico PLUS Chemiluminescent Substrate (ThermoFisher Scientific, 34580) and an LAS 3000 cooled CCD camera (Fujifilm, Tokyo, Japan).

2.8. CypA ELISA

The protein concentrations were determined with the BCA protein assay and adapted for microplates. The levels of CypA in the nuclear fraction were measured with commercially available kits according to the manufacturer's instructions (abx585050, Abxexa, Cambridge, UK). The absorbance was read on a microplate reader (Molecular Devices Corp., Sunnyvale, CA, USA), and the concentration was expressed as $\mu\text{g}/\text{mg}$ protein.

2.9. Statistical analysis

The Statistical Package for the Social Sciences 22.0 (SPSS, IBM, NY, USA) and GraphPad Prism 8 Software (GraphPad Software, San Diego, CA, USA) were used for all of the analyses. Comparisons between groups were performed by Student's *t*-test, and two-way ANOVA was used for multiple comparisons (LSD and Bonferroni tests) when equal

variances between groups were assumed. Data with unequal variance were compared with the Mann-Whitney *U* test. Results are presented as means \pm standard errors of the mean, and $p < 0.05$ was considered statistically significant.

3. Results

3.1. AIF(370-394)-TAT treatment reduces brain injury after HI

The short-term influence of the AIF(370-394)-TAT peptide treatment on brain injury in neonatal mice was evaluated by measuring the total infarction volume and neuropathological score at 72 h after HI based on the MAP2 immunostaining of brain sections (Fig. 2A). A total of 31 mice (16 females and 15 males) were treated with the AIF(370-394)-TAT peptide, and 31 mice (16 females and 15 males) were treated with vehicle and used as controls. The infarction volumes in AIF(370-394)-TAT-treated mice were 48.1% lower compared to vehicle-treated

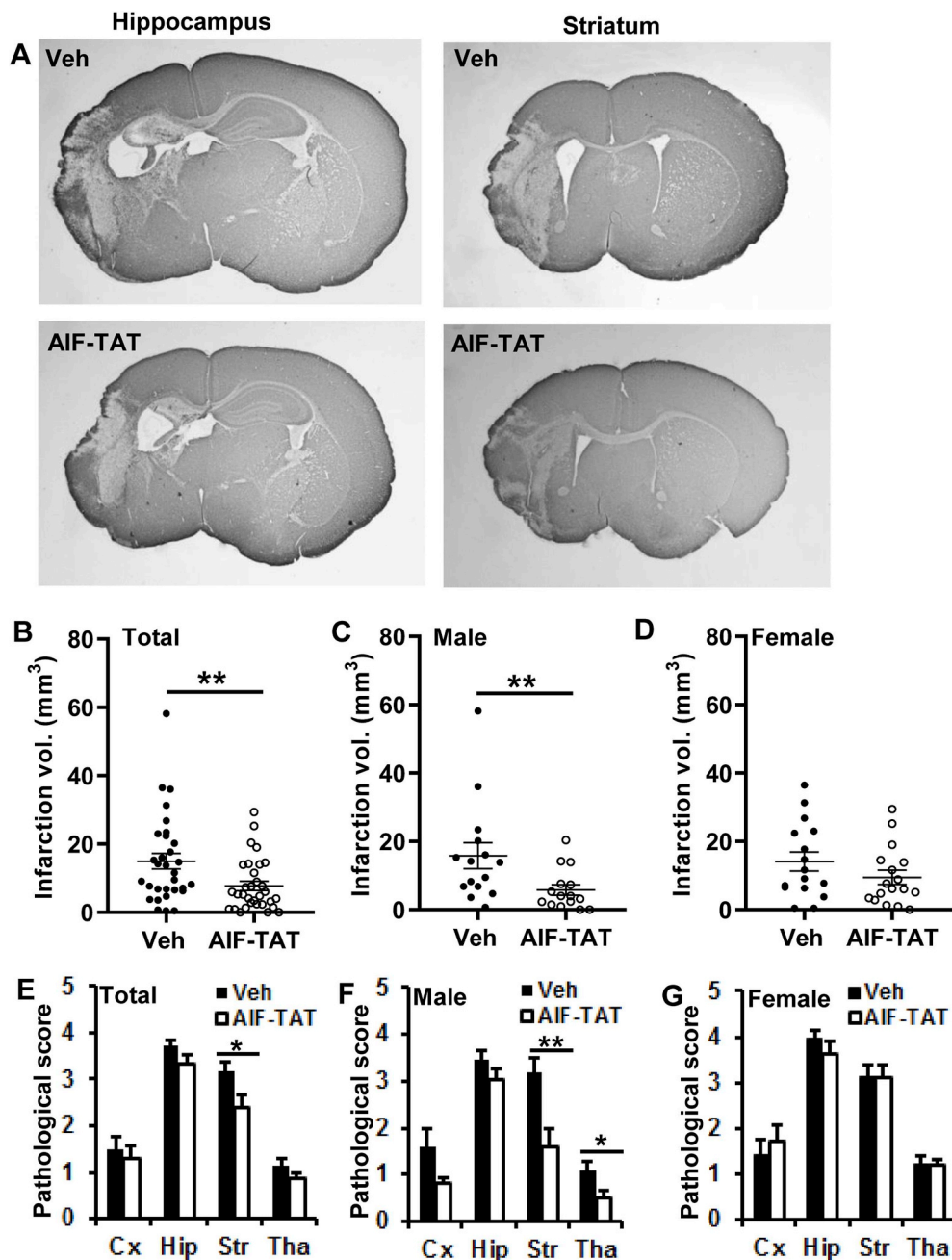


Fig. 2. AIF(370-394)-TAT treatment reduces brain injury in neonatal HI mice. **A.** Representative MAP2 staining of coronal brain sections at the hippocampus level (upper panels) and striatum level (lower panels) from vehicle and AIF(370-394)-TAT-treated mice at 72 h after HI. **B.** The infarction volume was measured at 72 h after HI in vehicle and AIF(370-394)-TAT-treated mice ($14.9 \text{ mm}^3 \pm 2.3$ vs. $7.8 \pm 1.3 \text{ mm}^3$, respectively, $n = 31/\text{group}$, $**p < 0.01$). **C.** The infarction volume measured at 72 h after HI only in males ($15.8 \pm 3.8 \text{ mm}^3$ for vehicle and $5.8 \pm 1.5 \text{ mm}^3$ for AIF-TAT, $n = 15/\text{group}$, $**p < 0.01$). **D.** The infarction volume measured at 72 h after HI only in females ($14.1 \pm 2.8 \text{ mm}^3$ for vehicle and $9.5 \pm 2.1 \text{ mm}^3$ for AIF-TAT, $n = 16/\text{group}$). **E.** The pathological scores evaluated in different brain regions in vehicle and AIF-TAT-treated mice, including the cortex (Cx, 1.5 ± 0.3 vs. 1.3 ± 0.3 , respectively), hippocampus (Hip, 3.7 ± 0.1 vs. 3.3 ± 0.2 , respectively), striatum (Str, 3.2 ± 0.2 vs. 2.4 ± 0.3 , respectively, $*p < 0.05$), and thalamus (Tha, 1.2 ± 0.1 vs. 0.9 ± 0.1 , respectively). **F.** The pathological scores evaluated in male mice in different brain regions in vehicle and AIF-TAT-treated mice, including the cortex (Cx, 1.6 ± 0.4 vs. 0.8 ± 0.1 , respectively), hippocampus (Hip, 3.5 ± 0.2 vs. 3.0 ± 0.3 , respectively), striatum (Str, 3.2 ± 0.3 vs. 1.6 ± 0.4 , respectively, $**p < 0.01$), and thalamus (Tha, 1.1 ± 0.2 vs. 0.5 ± 0.2 , respectively, $*p < 0.05$). **G.** The pathological scores evaluated in female mice in different brain regions in vehicle and AIF-TAT-treated mice, including the cortex (Cx, 1.4 ± 0.3 vs. 1.7 ± 0.4 , respectively), hippocampus (Hip, 3.9 ± 0.2 vs. 3.6 ± 0.3 , respectively), striatum (Str, 3.1 ± 0.3 vs. 3.1 ± 0.3 , respectively), and thalamus (Tha, 1.2 ± 0.2 vs. 1.2 ± 0.1 , respectively).

littermates ($p < 0.01$) (Fig. 2B). When analyzing the infarction volume segregated by sex, the average infarction volume was 63.3% lower in AIF (370-394)-TAT-treated male mice compared to vehicle-treated littermates ($p < 0.01$) (Fig. 2C). For females, the average values were 32.9% lower in AIF (370-394)-TAT-treated female mice compared to vehicle-treated littermates (Fig. 2D).

We further analyzed the different brain regions (cortex, hippocampus, striatum, and thalamus) and found that the decrease in the neuropathological score in AIF(370-394)-TAT-treated mice was only significant in the striatum (reduced by a 24.6%, $p < 0.05$), while there was only a non-significant tendency for a decrease in the cortex, hippocampus, and thalamus (Fig. 2E). This difference was more pronounced in male mice with reduced injury in both the striatum (50% decrease in neuropathological score in AIF(370-394)-TAT-treated male mice, $p < 0.01$) and the thalamus (reduced by 52.7%, $p < 0.05$), while only a tendency was observed in the cortex and hippocampus (Fig. 2F). No differences were observed in female mice in any of the specific brain regions examined ($p > 0.05$) (Fig. 2G).

In order to evaluate the potential protective effect of the AIF(370-394)-TAT peptide in the white matter, MBP staining was carried out as described at 72 h after HI (Fig. 3A). The MBP-positive area in the subcortical white matter zone of the ipsilateral hemisphere was separated from the contralateral hemisphere for each brain, and the extent of injury was measured and calculated as the ratio of the MBP-positive subcortical white matter in the ipsilateral hemisphere to that of the contralateral hemisphere. The ratio in AIF(370-394)-TAT-treated mice was 21.7% higher than in vehicle-treated mice ($p = 0.018$), meaning that the subcortical white matter was less injured in AIF(370-394)-

TAT-treated mice at 72 h post-HI (Fig. 3B). When taking into account the effect of sex, the ratio in males was 25.0% higher in AIF (370-394)-TAT-treated male mice compared to vehicle-treated male mice ($p < 0.05$) (Fig. 3C), whereas in females the difference was milder (17.4% increase in AIF (370-394)-TAT-treated female mice, $p > 0.05$) (Fig. 3D).

3.2. Impact of AIF(370-394)-TAT treatment on neuronal cell death after HI

Another group of mice was selected for investigating the effect of the peptide on neuronal cell death and microglia activation at 8 h and at 24 h after HI. For this purpose, only male mice were selected based on the above brain injury evaluation and the significant difference that was seen in male mice. Neuronal cell death in different brain regions (cortex, striatum, the CA1 sector of the hippocampus, and the NH) was investigated using Fluoro-Jade labeling, a non-specific neuronal cell death marker, at 8 h and 24 h after HI in neonatal male mouse brain (Fig. 4A). Fluoro-Jade-positive labeling was observed only in the injury area, and there was a general decrease in Fluoro-Jade-positive cells in AIF(370-394)-TAT-treated mice in the ipsilateral hemisphere compared to the ipsilateral hemisphere of vehicle-treated mice. The difference was statistically significant in the CA1 region of the hippocampus at 8 h post-HI ($p < 0.01$) and in the NH at 24 h post-HI ($p < 0.05$, $n = 5$ /group) (Fig. 4B). We then investigated caspase-dependent apoptotic cell death as indicated by active caspase-3 immunohistochemical labeling in brain sections (Fig. 5A). We found no significant differences between the AIF(370-394)-TAT and vehicle-treated male groups for any of the four brain regions studied at 8 h or 24 h after HI (Fig. 5B). We further

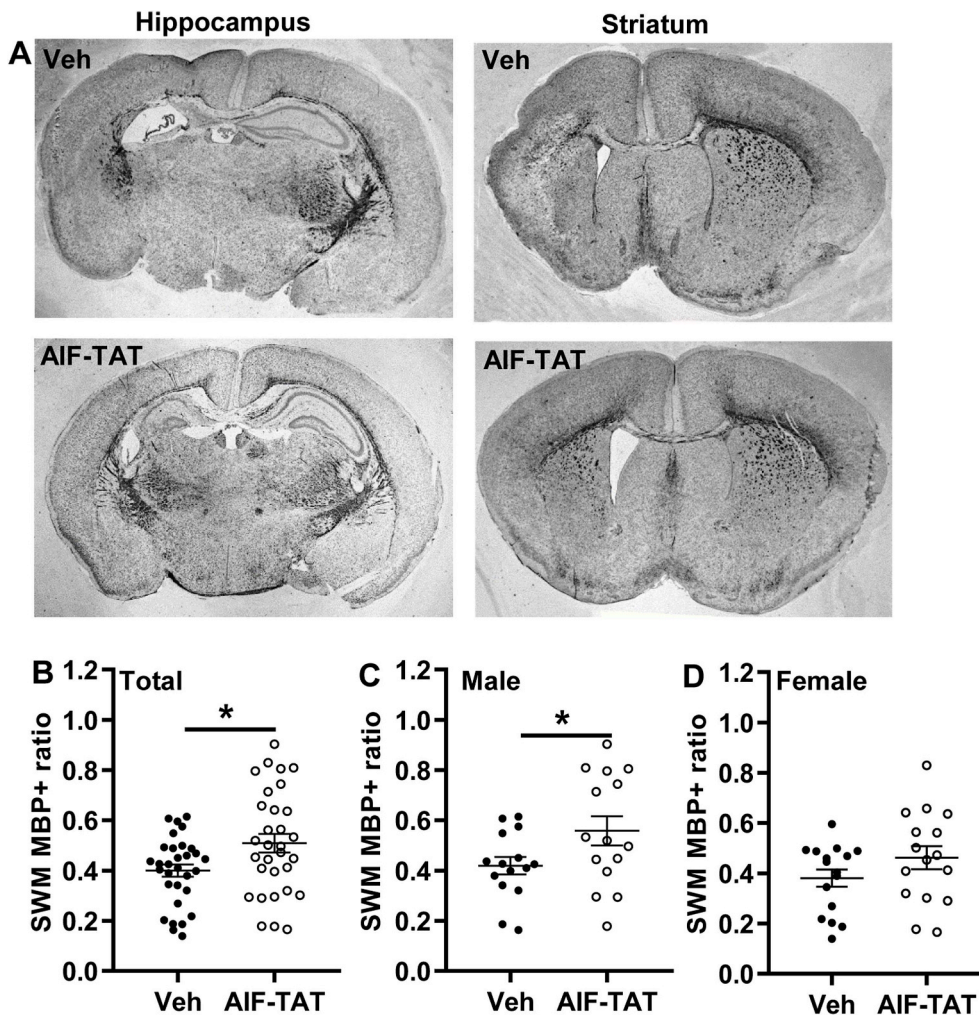


Fig. 3. AIF(370-394)-TAT treatment protects white matter in neonatal HI mice. **A.** Representative MBP staining of coronal brain sections revealed the myelin structure in the subcortical white matter of the contralateral and ipsilateral hemispheres at the hippocampus level (upper panels) and striatum level (lower panels) at 72 h after HI. **B.** The ratio of MBP-positive areas in the subcortical white matter (SWM) showed more white matter loss in vehicle-treated mice compared to AIF-TAT-treated mice at 72 h after HI (0.399 ± 0.025 vs. 0.51 ± 0.037 , $*p < 0.05$, $n = 31$ /group). **C.** The ratio of the MBP-positive areas in the SWM in vehicle-treated and AIF-TAT-treated male mice at 72 h after HI (0.42 ± 0.04 vs. 0.56 ± 0.06 , $*p < 0.05$, $n = 15$ /group). **D.** The ratio of the MBP-positive areas in the SWM in vehicle-treated and AIF-TAT-treated female mice at 72 h after HI (0.46 ± 0.06 vs. 0.46 ± 0.06 , respectively, $n = 16$ /group).

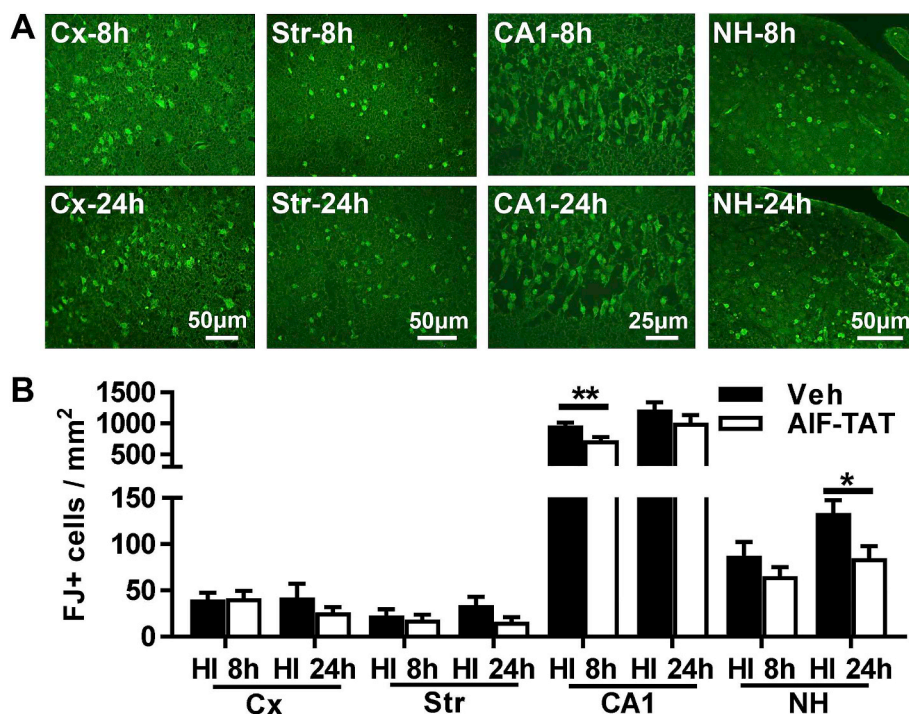


Fig. 4. AIF(370-394)-TAT treatment reduces the number of Fluoro-Jade-labeled cells.

A. Representative Fluoro-Jade staining in the cortex, striatum, CA1 of the hippocampus, and NH at 8 h and 24 h after HI. **B.** The bar graph shows the quantification of Fluoro-Jade-labeled cells in vehicle and AIF-TAT-treated male mice at 8 h and 24 h after HI in the cortex (40.3 ± 7.4 cells / mm² vs. 41.8 ± 7.6 cells / mm² at 8 h and 42.3 ± 15.6 cells / mm² vs. 26.3 ± 5.8 cells / mm² at 24 h after HI), striatum (23.1 ± 6.4 cells / mm² vs. 18.5 ± 5.2 cells / mm² at 8 h and 34.3 ± 9.0 cells / mm² vs. 16.4 ± 4.9 cells / mm² at 24 h after HI), CA1 (967.7 ± 48.0 cells / mm² vs. 728.6 ± 54.4 cells / mm² at 8 h ($p < 0.01$) and $1,225.0 \pm 114.2$ cells / mm² vs. $1,013.0 \pm 124.7$ cells / mm² at 24 h after HI), and NH (87.5 ± 15.0 cells / mm² vs. 65.7 ± 9.5 cells / mm² at 8 h and 133.7 ± 13.7 cells / mm² vs. 85.0 ± 12.9 cells / mm² at 24 h after HI ($p < 0.05$)). * $p < 0.05$; ** $p < 0.01$; n = 5/group.

investigated caspase-independent apoptotic cell death using AIF immunohistochemical staining in which AIF-positive cells show positive staining in the nucleus (Fig. 6A). The numbers of AIF-positive nuclei counted in AIF(370-394)-TAT-treated male mice decreased significantly in the cortex, striatum, and NH at 8 h after HI compared to vehicle-treated male mice ($p < 0.05$). At 24 h post-HI, however, the results showed a non-significant tendency for lower numbers of AIF-positive nuclei in the AIF(370-394)-TAT-treated male mice compared to vehicle-treated male mice ($p > 0.05$) (Fig. 6B).

3.3. AIF(370-394)-TAT treatment has no significant effects on microglia activation

Microglia activation and inflammation have been shown to be related with perinatal HI brain injury (Xie et al., 2014). To determine if the AIF(370-394)-TAT peptide has an effect on microglia activation, we analyzed galectin-3-positive cells, which is a marker of pathologically activated microglia (Li et al., 2011). Galectin-3-positive cells were detected in the ipsilateral hemisphere at 8 h after HI (Fig. 7A), and this number increased dramatically at 24 h after HI (Fig. 7B). The number of

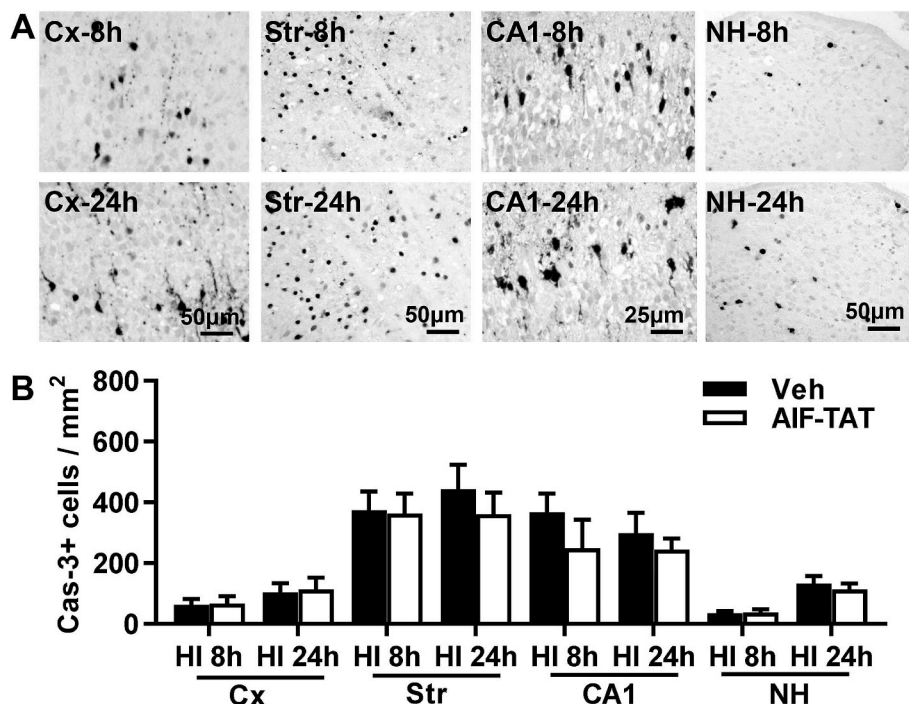


Fig. 5. AIF(370-394)-TAT treatment has no impact on caspase-3 activation.

A. Representative active caspase-3 staining in the cortex, striatum, CA1, and NH of the ipsilateral hemisphere at 8 h and 24 h after HI. **B.** The bar graph shows the quantification of active caspase-3-positive cells in vehicle and AIF-TAT-treated mice at 8 h and 24 h after HI in the cortex (63.2 ± 19.2 cells / mm² vs. 67.4 ± 23.5 cells / mm² at 8 h and 103.7 ± 30.7 cells / mm² vs. 113.0 ± 39.4 cells / mm² at 24 h after HI), striatum (374.9 ± 60.5 cells / mm² vs. 362.9 ± 65.8 cells / mm² at 8 h and 443.0 ± 80.3 cells / mm² vs. 360.7 ± 71.6 cells / mm² at 24 h after HI), CA1 (368.3 ± 60.6 cells / mm² vs. 249.1 ± 94.2 cells / mm² at 8 h and 299.3 ± 65.9 cells / mm² vs. 244.8 ± 35.7 cells / mm² at 24 h after HI), and NH (35.6 ± 6.4 cells / mm² vs. 38.0 ± 9.8 cells / mm² at 8 h and 133.0 ± 24.1 cells / mm² vs. 113.8 ± 18.9 cells / mm² at 24 h after HI). n = 5/group.

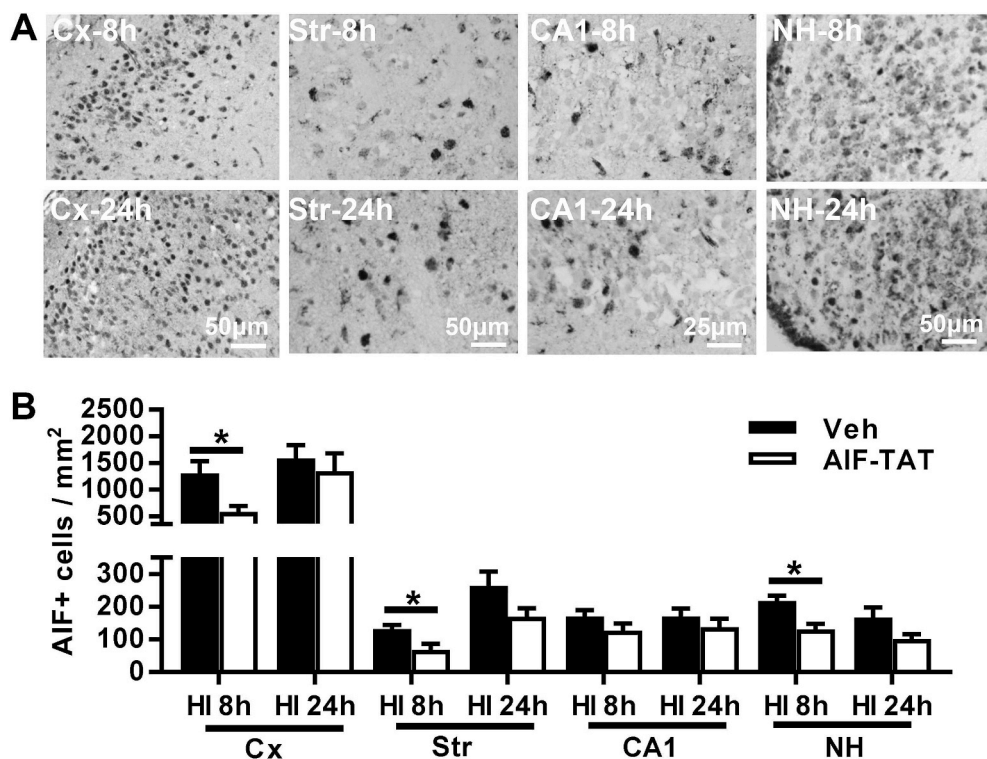


Fig. 6. AIF(370-394)-TAT treatment reduces AIF translocation to the nucleus after HI.

A. Representative AIF immunostaining in the cortex, striatum, CA1, and NH of the ipsilateral hemisphere at 8 h and 24 h. **B.** The bar graph shows the quantification of AIF-positive nuclei / mm² in vehicle and AIF-TAT-treated mice at 8 h and at 24 h after HI in the cortex (1,310.0 ± 226.7 nuclei vs. 586.4 ± 109.7 nuclei at 8 h, and 1,588.0 ± 245.0 nuclei vs. 1,350.0 ± 320.8 nuclei at 24 h after HI), striatum (131.6 ± 12.6 nuclei vs. 68.9 ± 17.4 nuclei at 8 h and 263.4 ± 43.6 nuclei vs. 168.8 ± 17.4 nuclei at 24 h after HI), CA1 (170.7 ± 18.7 nuclei vs. 127.8 ± 21.6 nuclei at 8 h and 170.7 ± 23.7 nuclei vs. 137.4 ± 26.6 nuclei at 24 h after HI), and NH (218.1 ± 16.1 nuclei vs. 130.8 ± 17.5 nuclei at 8 h post-HI and 167.0 ± 30.4 nuclei vs. 101.7 ± 14.8 nuclei at 24 h after HI). **p* < 0.05, *n* = 5/group.

galectin-3-positive cells was decreased slightly in the AIF(370-394)-TAT-treated group compared to the vehicle-treated group at both 8 h and 24 h after HI in the cortex and striatum, but the difference was not significant (Fig. 7).

3.4. AIF(370-394)-TAT treatment has no significant effect on mitochondrial biogenesis

To investigate the impact of AIF(370-394)-TAT treatment on mitochondrial cell death-related proteins after HI, the mitochondrial intermembrane space protein expression of AIF, cytochrome c, and CHCHD4 were measured in the mitochondrial fraction at 8 h and 24 h after HI (Fig. 8A). The protein expression was decreased in the ipsilateral hemisphere after HI, and this was more pronounced at 24 h after HI. However, the quantification did not show significant differences between vehicle and AIF(370-394)-TAT treatment groups even though there was a tendency for more proteins to be released from the mitochondria in the ipsilateral hemisphere of the vehicle treatment group (data not shown). To further determine if AIF(370-394)-TAT peptide treatment has an impact on mitochondrial biogenesis, the five membrane-bound protein complexes (I: NADH-ubiquinone oxidoreductase; II: succinate-ubiquinone oxidoreductase; III: ubiquinone cytochrome c; IV: cytochrome c oxidase; V: ATP synthase) that catalyze oxidative phosphorylation (OxPhos) in the mitochondria were measured in the mitochondrial fraction at 8 h and 24 h after HI (Fig. 8B). The quantification of the complexes did not show significant changes in the ipsilateral hemisphere at either 8 h or 24 h after AIF(370-394)-TAT treatment (data not shown).

3.5. AIF(370-394)-TAT treatment inhibits AIF nuclear translocation after HI

In order to prove that the AIF(370-394)-TAT peptide was actually blocking AIF translocation from the cytosol to the nucleus, we performed two independent experiments. First, we analyzed the protein expression of AIF in neonatal male mice by immunoblotting in the nuclear fraction extracted from the total brain homogenate at 8 h and at

24 h after HI (Fig. 9A). AIF accumulation in the nuclear fraction was increased with longer time after the HI insult, and it was 3.6 times higher at 24 h compared to 8 h after HI in the vehicle-treated group. There was a tendency for less AIF accumulation in the nucleus at 8 h post-HI in the AIF(370-394)-TAT-treated group compared to the vehicle-treated group. The difference was much more pronounced at 24 h post-HI, meaning that AIF (370-394)-TAT treatment prevented AIF accumulation in the nucleus compared to vehicle treatment (*p* < 0.05) (Fig. 9B).

Second, we examined CypA expression in the nuclear fraction in neonatal male mice by immunoblotting and ELISA. The immunoblotting results showed similar patterns for CypA and AIF when quantifying the immunoblotting bands. At 8 h post-HI, there was no significant difference between the AIF(370-394)-TAT treatment and the vehicle treatment. At 24 h post-HI, CypA expression increased in the nuclear fraction compared to 8 h post-HI, and AIF (370-394)-TAT treatment reduced the expression of CypA in the nucleus, meaning that AIF(370-394)-TAT treatment prevented CypA accumulation in the nucleus (*p* < 0.01) (Fig. 9C). ELISA analysis of CypA in the nuclear fraction showed lower CypA (29.6% reduction; *p* < 0.05) at 8 h post-HI after AIF (370-394)-TAT treatment, and the reduction in CypA became even greater at 24 h after HI, with a 55% reduction in AIF(370-394)-TAT-treated mice compared to vehicle-treated mice (*p* < 0.05) (Fig. 9D).

4. Discussion

Apoptotic cell death plays a more prominent role in the immature brain compared to the adult brain under pathological conditions such as cerebral HI (Zhu et al., 2005), and we previously showed that AIF-mediated caspase-independent apoptosis is positively correlated with brain injury in the immature brain after HI (Zhu et al., 2003). This indicates that AIF plays an important role in the process of neuronal cell death and brain injury in the immature brain after injury. In this study, we used the cell-penetrating AIF(370-394)-TAT peptide to block the formation of the AIF/CypA complex in our neonatal mouse cerebral HI model, thus reducing neuronal cell death and brain injury, and this effect was more pronounced in males.

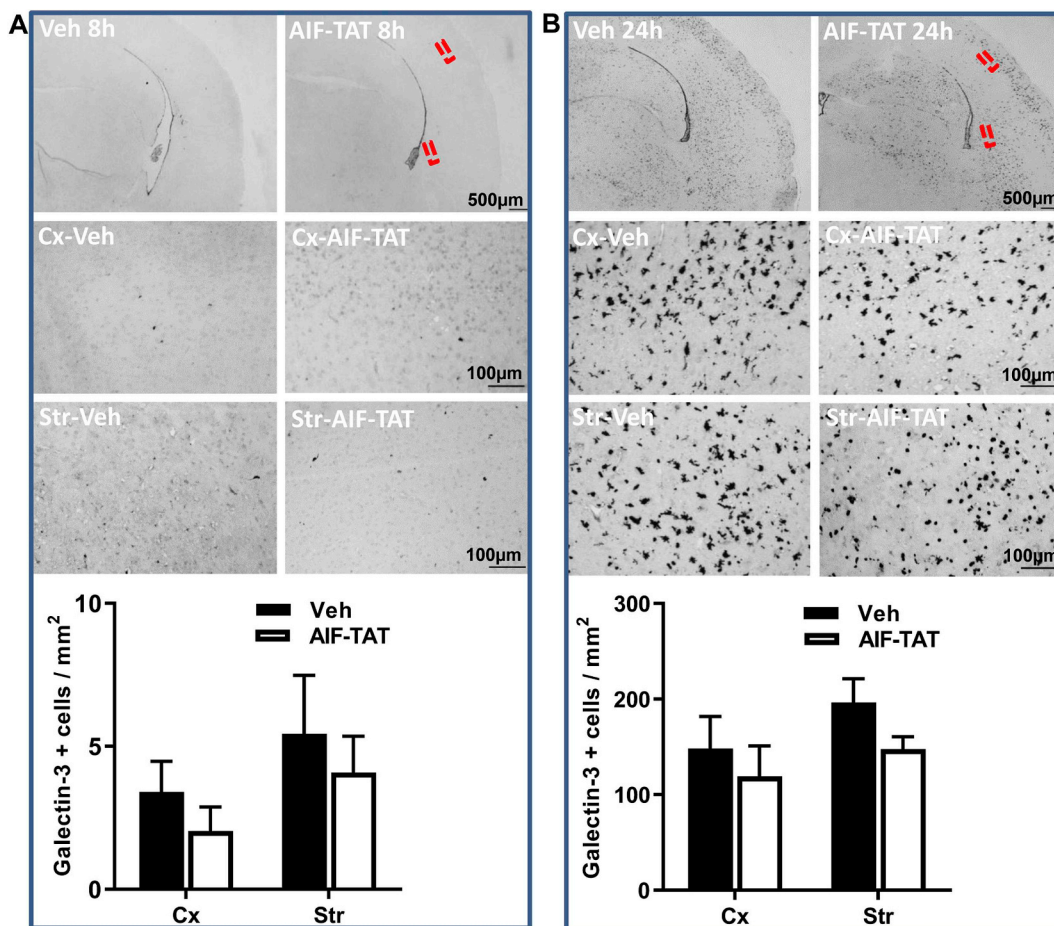


Fig. 7. AIF(370-394)-TAT treatment has no significant influence on microglia activation.

A. Representative overview (top panel), cortex (middle panel), and striatum (lower panel) galectin-3 immunostaining in the ipsilateral hemisphere at 8 h after HI in both vehicle and AIF(370-394)-TAT-treated mice. The bar graph shows quantification of the galectin-3-positive cells in the cortex and striatum. The number of positive cells was not significantly different with AIF (370-394)-TAT treatment. B. Representative overview (top panel), cortex (middle panel), and striatum (lower panel) galectin-3 immunostaining in the ipsilateral hemisphere at 24 h after HI. The number of positive cells increased dramatically compared with 8 h after HI. The bar graph shows the quantification of the galectin-3-positive cells in the cortex and striatum, and no difference was observed between the vehicle and AIF(370-394)-TAT treatment groups. n = 5/group.

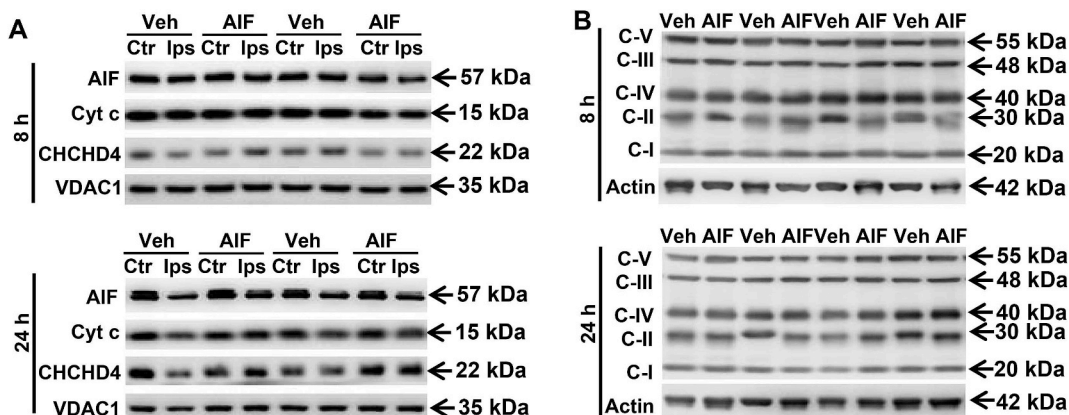


Fig. 8. AIF(370-394)-TAT treatment has no significant effect on mitochondrial cell death-related proteins or biogenesis.

A. Representative immunoblotting of AIF, cytochrome c, and CHCHD4 in the mitochondrial fraction of cortical tissue from the contralateral hemisphere (Ctr) and ipsilateral hemisphere (Ips) of vehicle (Veh) and AIF(370-394)-TAT treatment at 8 h (up panel) and 24 h (lower panel) after HI. B. Representative immunoblotting of OxPhos including all five membrane-bound protein complexes in the mitochondrial fraction of the ipsilateral hemisphere at 8 h (up panel) and 24 h (lower panel) after HI. There was no significant difference between the two treatment groups. n = 6/group.

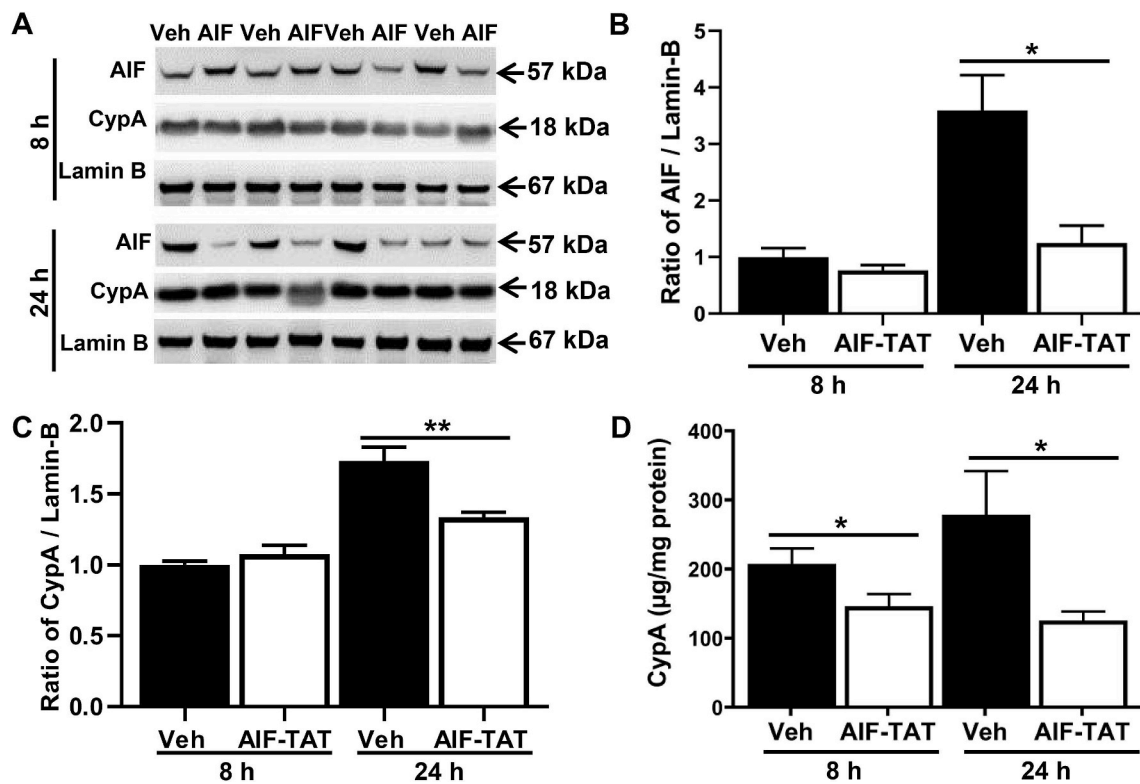


Fig. 9. AIF(370-394)-TAT treatment reduces AIF/CypA translocation to the nucleus after HI. **A.** Representative AIF and CypA immunoblotting from the nuclear fraction of the cortical tissue in the ipsilateral hemisphere of vehicle and AIF-TAT-treated mice at 8 h and at 24 h after HI. **B.** Quantification of AIF immunoblotting in the nuclear fraction from the ipsilateral hemisphere of vehicle and AIF-TAT-treated male mice at 8 h and 24 h after HI. AIF-TAT treatment reduced AIF accumulation in the nucleus at 24 h after HI by 65% compared to vehicle treatment (**p* < 0.05, *n* = 6/group). **C.** Quantification of CypA protein in the nuclear fraction from the ipsilateral hemisphere of vehicle and AIF-TAT-treated male mice at 8 h and 24 h after HI. CypA accumulation in the nucleus increased at 24 h compared to 8 h after HI, and AIF-TAT treatment reduced CypA accumulation in the nucleus by 21.6% (***p* < 0.01, *n* = 6/group). **D.** ELISA analysis of CypA in the nuclear fraction of cortical tissue from the ipsilateral hemisphere of vehicle and AIF-TAT-treated mice at 8 h (207.5 ± 22.4 µg/mg vs. 146.0 ± 17.9 µg/mg) and at 24 h after HI (278.6 µg/mg ± 63.0 vs. 125.6 ± 12.9 µg/mg protein). **p* < 0.05, *n* = 6/group.

AIF is a flavin adenine dinucleotide-dependent NADH oxidoreductase that resides in the mitochondria under physiological conditions, and two isoforms have been identified – the ubiquitously expressed AIF1 and the brain-specific AIF2 (Hangen et al., 2010). AIF also regulates the assembly and maintenance of the respiratory complexes in mitochondria, thus influencing metabolic pathways (Bano and Prehn, 2018), and AIF deficiency leads to mitochondria dysfunction and neurodegeneration (Klein et al., 2002). However, studies have shown that AIF also plays a central role in neuronal cell death under pathological conditions (Zhu et al., 2007a; Culmsee et al., 2005), and in response to apoptosis-inducing stimuli AIF is released from the mitochondria and translocates to the nucleus where it induces chromatinolysis and DNA fragmentation. The mechanism by which AIF translocates to the nucleus has been the matter of some debate (Zhu et al., 2007b; Doti et al., 2014; Artus et al., 2010). It has been suggested that AIF and CypA independently translocate into the nucleus, which is supported by the results in a necrosis model in which CypA down-regulation did not compromise the nuclear translocation of AIF but reduced DNA damage (Artus et al., 2010). It has also been suggested that AIF and CypA form a complex in the cytosol and that this interaction allows both proteins to translocate into the nucleus and induce cell death (Cande et al., 2004). This hypothesis was supported by the observation that nuclear translocation of AIF after HI was significantly reduced in CypA^{-/-} mice compared to wild-type littermates and that AIF-blocking peptide inhibited AIF/CypA complex formation and protected against oxidative stress-induced neuronal cell death (Zhu et al., 2007b; Doti et al., 2014). Here we show that our AIF (370-394)-TAT peptide reduced both AIF and CypA expression in the nuclear fraction after HI, but not AIF release from mitochondria, which is consistent with reduced neuronal cell

death and reduced brain injury. These results suggest that the AIF/CypA complex is essential for HI-induced cell death and brain injury in the immature brain, at least in males.

Sex differences in perinatal brain injury have been previously reported in different studies (Li et al., 2019; Bi et al., 2014; Zhu et al., 2013; Narang et al., 2019). These results suggest that sex might play a modulatory role in neuronal cell death and brain injury, which might be related to intrinsic sex differences, but not related to circulating gonadal hormones (Charriaut-Marlangue et al., 2017; Du et al., 2004), including differential gene expression (Dewing et al., 2003). Our previous study showed that different apoptotic mechanisms are activated in male and female mouse brains after cerebral HI, and the AIF pathway is more prominent in males and the caspase-dependent apoptotic cell death pathway is more prominent in females (Zhu et al., 2006). Furthermore, a previous study also showed that mitochondrial respiratory impairment and oxidative stress after neonatal HI are more obvious in males than in females (Demarest et al., 2016). Another study showed that poly (ADP-ribose) polymerase-1 (PARP-1) is a mediator of caspase-independent apoptotic cell death after ischemia-reperfusion injury, and AIF release from mitochondria into the nucleus is required for PARP-1 activation (Yu et al., 2002). In addition, genetic deletion of PARP-1 is preferentially protective against perinatal brain injury in males (Hagberg et al., 2004). The degree of PAR accumulation during the first hours (1–4 h) after HI was similar in female and male P7 mice, but there was a drop in NAD⁺ in males, but not in females. There are other studies reporting sex differences when using hypothermia after HI, resulting in more effective long-term protection in female than in male 7-day-old rats (Bona et al., 1998). All of these studies indicate that AIF-induced cell death is sex related (Renolleau et al., 2008). In this paper

we have shown again that the AIF apoptotic pathway is more prevalent in males than in females because the AIF-blocking peptide showed greater protection in male mice.

In summary, the administration of the AIF (370-394)-TAT peptide prevents AIF/CypA translocation into the nucleus, protects against caspase-independent apoptotic neuron death, and protects the neonatal brain after HI-induced injury in male mice. These results suggest that the AIF/CypA complex might be a therapeutic target for neuroprotection in the immature brain.

Declaration of conflicting interests

The authors declare no potential conflicts of interest with respect to the research, authorship, or publication of this article.

CRedit authorship contribution statement

Juan Rodriguez: Data curation, Writing - original draft. **Cuicui Xie:** Methodology. **Tao Li:** Validation, Data curation. **Yanyan Sun:** Data curation. **Yafeng Wang:** Data curation, Validation. **Yiran Xu:** Visualization. **Kenan Li:** Data curation. **Shan Zhang:** Data curation. **Kai Zhou:** Investigation. **Yong Wang:** Data curation. **Carina Mallard:** Writing - review & editing, Supervision. **Henrik Hagberg:** Writing - review & editing, Supervision. **Nunzianna Doti:** Resources, Writing - review & editing. **Xiaoyang Wang:** Visualization, Formal analysis, Writing - review & editing. **Changlian Zhu:** Conceptualization, Methodology, Funding acquisition, Project administration, Supervision.

Acknowledgments

This work was supported by the Swedish Research Council (2018-02667, 2019-01320), the National Natural Science Foundation of China (31761133015, U1704281, 81901335), the Swedish Childhood Cancer Foundation (PR2016-072, NCP2016-0019, PR2018-0082), the Swedish Cancer Foundation (CAN2017/509), Swedish Governmental grants to scientists working in health care (ALFGBG-717791, 137601), the Wilhelm and Martina Lundgren Foundation (2016-1066, 2017-1734), the Swedish Brain Foundation (FO2018-0034), the Department of Science and Technology of Henan Province, China (171100310200), and the Chinese Scholarship Council to TL (201707040025), YW (201807040027), and YX (201507040082).

Appendix A. Supplementary data

Supplementary data to this article can be found online at <https://doi.org/10.1016/j.neuropharm.2020.108088>.

References

Albertsson, A.M., Zhang, X., Leavenworth, J., Bi, D., Nair, S., Qiao, L., et al., 2014. The effect of osteopontin and osteopontin-derived peptides on preterm brain injury. *J. Neuroinflammation* 11, 197.

Artus, C., Boujrad, H., Bouharrou, A., Brunelle, M.N., Hoos, S., Yuste, V.J., et al., 2010. AIF promotes chromatinolysis and caspase-independent programmed necrosis by interacting with histone H2AX. *EMBO J.* 29 (9), 1585–1599.

Azzopardi, D., Strohm, B., Marlow, N., Brocklehurst, P., Deierl, A., Eddama, O., et al., 2014. Effects of hypothermia for perinatal asphyxia on childhood outcomes. *N. Engl. J. Med.* 371 (2), 140–149.

Bano, D., Prehn, J.H.M., 2018. Apoptosis-inducing factor (AIF) in physiology and disease: the tale of a repented natural born killer. *EBioMedicine* 30, 29–37.

Bi, D., Chen, M., Zhang, X., Wang, H., Xia, L., Shang, Q., et al., 2014. The association between sex-related interleukin-6 gene polymorphisms and the risk for cerebral palsy. *J. Neuroinflammation* 11, 100.

Bona, E., Hagberg, H., Löberg, E.M., Bågenholm, R., Thoresen, M., 1998. Protective effects of moderate hypothermia after neonatal hypoxia-ischemia: short- and long-term outcome. *Pediatr. Res.* 43 (6), 738–745.

Cande, C., Vahsen, N., Kouranti, I., Schmitt, E., Daugas, E., Spahr, C., et al., 2004. AIF and cyclophilin A cooperate in apoptosis-associated chromatinolysis. *Oncogene* 23 (8), 1514–1521.

Charriaut-Marlangue, C., Besson, V.C., Baud, O., 2017. Sexually dimorphic outcomes after neonatal stroke and hypoxia-ischemia. *Int. J. Mol. Sci.* 19 (1), E61.

Culmsee, C., Zhu, C., Landshamer, S., Becattini, B., Wagner, E., Pellecchia, M., et al., 2005. Apoptosis-inducing factor triggered by poly(ADP-ribose) polymerase and Bid mediates neuronal cell death after oxygen-glucose deprivation and focal cerebral ischemia. *J. Neurosci.* 25 (44), 10262–10272.

Demarest, T.G., Schuh, R.A., Waddell, J., McKenna, M.C., Fiskum, G., 2016. Sex-dependent mitochondrial respiratory impairment and oxidative stress in a rat model of neonatal hypoxic-ischemic encephalopathy. *J. Neurochem.* 137 (5), 714–729.

Dewing, P., Shi, T., Horvath, S., Vilain, E., 2003. Sexually dimorphic gene expression in mouse brain precedes gonadal differentiation. *Mol. Brain Res.* 118 (1–2), 82–90.

Doti, N., Reuther, C., Scognamiglio, P.L., Dolga, A.M., Plesnila, N., Ruvo, M., et al., 2014. Inhibition of the AIF/CypA complex protects against intrinsic death pathways induced by oxidative stress. *Cell Death Dis.* 5, e993.

Du, L., Bayir, H., Lai, Y., Zhang, X., Kochanek, P.M., Watkins, S.C., et al., 2004. Innate gender-based proclivity in response to cytotoxicity and programmed cell death pathway. *J. Biol. Chem.* 279 (37), 38563–38570.

Farina, B., Di Sorbo, G., Chambery, A., Caporale, A., Leoni, G., Russo, R., et al., 2017. Structural and biochemical insights of CypA and AIF interaction. *Sci. Rep.* 7 (1), 1138.

Fleiss, B., Gressens, P., 2012. Tertiary mechanisms of brain damage: a new hope for treatment of cerebral palsy? *Lancet Neurol.* 11 (6), 556–566.

Hagberg, H., Wilson, M.A., Matsushita, H., Zhu, C., Lange, M., Gustavsson, M., et al., 2004. PARP-1 gene disruption in mice preferentially protects males from perinatal brain injury. *J. Neurochem.* 90 (5), 1068–1075.

Hagberg, H., Mallard, C., Rousset, C.I., Thornton, C., 2014. Mitochondria: hub of injury responses in the developing brain. *Lancet Neurol.* 13 (2), 217–232.

Hagberg, H., David Edwards, A., Groenendaal, F., 2016. Perinatal brain damage: the term infant. *Neurobiol. Dis.* 92 (Pt A), 102–112.

Hangen, E., De Zio, D., Bordin, M., Zhu, C., Dessen, P., Caffin, F., et al., 2010. A brain-specific isoform of mitochondrial apoptosis-inducing factor: AIF2. *Cell Death Differ.* 17 (7), 1155–1166.

Klein, J.A., Longo-Guess, C.M., Rossmann, M.P., Seburn, K.L., Hurd, R.E., Frankel, W.N., et al., 2002. The harlequin mouse mutation downregulates apoptosis-inducing factor. *Nature* 419 (6905), 367–374.

Li, H., Li, Q., Du, X., Sun, Y., Wang, X., Kroemer, G., et al., 2011. Lithium-mediated long-term neuroprotection in neonatal rat hypoxia-ischemia is associated with anti-inflammatory effects and enhanced proliferation and survival of neural stem/progenitor cells. *J. Cerebr. Blood Flow Metabol.* 31 (10), 2106–2115.

Li, K., Li, T., Wang, Y., Xu, Y., Zhang, S., Culmsee, C., et al., 2019. Sex differences in neonatal mouse brain injury after hypoxia ischemia and adaptaquin treatment. *J. Neurochem.* 150 (6), 759–775.

Li, T., Li, K., Zhang, S., Wang, Y., Xu, Y., Cronin, S.J., et al., 2020. Overexpression of apoptosis inducing factor aggravates hypoxic-ischemic brain injury in neonatal mice. *Cell Death Dis.* 11 (1), 77.

Liu, L., Oza, S., Hogan, D., Chu, Y., Perin, J., Zhu, J., et al., 2016. Global, regional, and national causes of under-5 mortality in 2000–15: an updated systematic analysis with implications for the Sustainable Development Goals. *Lancet* 388 (10063), 3027–3035.

Narang, R., Carter, K., Muncie, C., Pang, Y., Fan, L.W., Feng, Y., et al., 2019. Intrauterine growth restriction and neonatal hypoxic ischemic brain injury causes sex-specific long-term neurobehavioral abnormalities in rats. *J. Neurosci. Res.* 97 (6), 661–672.

Natalucci, G., Latal, B., Koller, B., Ruegger, C., Sick, B., Held, L., et al., 2016. Effect of early prophylactic high-dose recombinant human erythropoietin in very preterm infants on neurodevelopmental outcome at 2 years: a randomized clinical trial. *J. Am. Med. Assoc.* 315 (19), 2079–2085.

Novak, C.M., Ozen, M., Burd, I., 2018. Perinatal brain injury: mechanisms, prevention, and outcomes. *Clin. Perinatol.* 45 (2), 357–375.

Renolleau, S., Fau, S., Charriaut-Marlangue, C., 2008. Gender-related differences in apoptotic pathways after neonatal cerebral ischemia. *Neuroscientist* 14 (1), 46–52.

Rodriguez, J., Zhang, Y., Li, T., Xie, C., Sun, Y., Xu, Y., et al., 2018. Lack of the brain-specific isoform of apoptosis-inducing factor aggravates cerebral damage in a model of neonatal hypoxia-ischemia. *Cell Death Dis.* 10 (1), 3.

Song, J., Sun, H., Xu, F., Kang, W., Gao, L., Guo, J., et al., 2016. Recombinant human erythropoietin improves neurological outcomes in very preterm infants. *Ann. Neurol.* 80 (1), 24–34.

Strunk, T., Inder, T., Wang, X., Burgner, D., Mallard, C., Levy, O., 2014. Infection-induced inflammation and cerebral injury in preterm infants. *Lancet Infect. Dis.* 14 (8), 751–762.

Sun, Y., Zhang, Y., Wang, X., Blomgren, K., Zhu, C., 2012. Apoptosis-inducing factor downregulation increased neuronal progenitor, but not stem cell, survival in the neonatal hippocampus after cerebral hypoxia-ischemia. *Mol. Neurodegener.* 7, 17.

Sun, Y., Li, T., Xie, C., Xu, Y., Zhou, K., Rodriguez, J., et al., 2017. Haploinsufficiency in the mitochondrial protein CHCHD4 reduces brain injury in a mouse model of neonatal hypoxia-ischemia. *Cell Death Dis.* 8 (5), e2781.

Thornton, C., Leaw, B., Mallard, C., Nair, S., Jinnai, M., Hagberg, H., 2017. Cell death in the developing brain after hypoxia-ischemia. *Front. Cell. Neurosci.* 11, 248.

Wu, Y., Song, J., Wang, Y., Wang, X., Culmsee, C., Zhu, C., 2019. The Potential role of ferroptosis in neonatal brain injury. *Front. Neurosci.* 13, 115.

Xie, C., Zhou, K., Wang, X., Blomgren, K., Zhu, C., 2014. Therapeutic benefits of delayed lithium administration in the neonatal rat after cerebral hypoxia-ischemia. *PLoS One* 9 (9), e107192.

Xie, C., Ginet, V., Sun, Y., Koike, M., Zhou, K., Li, T., et al., 2016. Neuroprotection by selective neuronal deletion of Atg7 in neonatal brain injury. *Autophagy* 12 (2), 410–423.

Yu, S.-W., Wang, H., Poitras, M.F., Coombs, C., Bowers, W.J., Federoff, H.J., et al., 2002. Mediation of poly (ADP-ribose) polymerase-1-dependent cell death by apoptosis-inducing factor. *Science* 297 (5579), 259–263.

- Zhu, C., Qiu, L., Wang, X., Hallin, U., Cande, C., Kroemer, G., et al., 2003. Involvement of apoptosis-inducing factor in neuronal death after hypoxia-ischemia in the neonatal rat brain. *J. Neurochem.* 86 (2), 306–317.
- Zhu, C., Wang, X., Xu, F., Bahr, B., Shibata, M., Uchiyama, Y., et al., 2005. The influence of age on apoptotic and other mechanisms of cell death after cerebral hypoxia-ischemia. *Cell Death Differ.* 12 (2), 162–176.
- Zhu, C., Xu, F., Wang, X., Shibata, M., Uchiyama, Y., Blomgren, K., et al., 2006. Different apoptotic mechanisms are activated in male and female brains after neonatal hypoxia-ischaemia. *J. Neurochem.* 96 (4), 1016–1027.
- Zhu, C., Wang, X., Huang, Z., Qiu, L., Xu, F., Vahsen, N., et al., 2007a. Apoptosis-inducing factor is a major contributor to neuronal loss induced by neonatal cerebral hypoxia-ischemia. *Cell Death Differ.* 14 (4), 775–784.
- Zhu, C., Wang, X., Deinum, J., Huang, Z., Gao, J., Modjtahedi, N., et al., 2007b. Cyclophilin A participates in the nuclear translocation of apoptosis-inducing factor in neurons after cerebral hypoxia-ischemia. *J. Exp. Med.* 204 (8), 1741–1748.
- Zhu, C., Kang, W., Xu, F., Cheng, X., Zhang, Z., Jia, L., et al., 2009. Erythropoietin improved neurologic outcomes in newborns with hypoxic-ischemic encephalopathy. *Pediatrics* 124 (2), e218.
- Zhu, C., Sun, Y., Gao, J., Wang, X., Plesnila, N., Blomgren, K., 2013. Inhaled nitric oxide protects males but not females from neonatal mouse hypoxia-ischemia brain injury. *Transl Stroke Res* 4 (2), 201–207.